Received 31 December 2009
Revised 3 May 2010,
29 July 2010,
7 October 2010
Accepted 28 October 2010

Efficient simulations of detailed combustion fields via the lattice Boltzmann method

Eliodoro Chiavazzo
Politecnico di Torino, Torino, Italy
Ilya V. Karlin
Swiss Federal Institute of Technology (ETH), Zurich, Switzerland
Alexander N. Gorban
University of Leicester, Leicester, UK, and
Konstantinos Boulouchos
Swiss Federal Institute of Technology (ETH), Zurich, Switzerland

Abstract

Purpose – The paper aims to be a first step toward the efficient, yet accurate, solution of detailed combustion fields using the lattice Boltzmann (LB) method, where applications are still limited due to both the stiffness of the governing equations and the large amount of fields to solve.

Design/methodology/approach – The suggested methodology for model reduction is developed in the setting of slow invariant manifold construction, including details of the while. The simplest LB equation is used in order to work out the procedure of coupling of the reduced model with the flow solver.

Findings – The proposed method is validated with the 2D simulation of a premixed laminar flame in the hydrogen-air mixture, where a remarkable computational speedup and memory saving are demonstrated.

Research limitations/implications – Because of the chosen detailed LB model, the flow field may be described with unsatisfactory accuracy: this motivates further investigation in this direction in the near future.

Practical implications – A new framework of simulation of reactive flows is available, based on a coupling between accurate reduced reaction mechanism and the LB representation of the flow phenomena. Hence, the paper includes implications on how to perform accurate reactive flow simulations at a fraction of the cost required in the detailed model.

Originality/value – This paper meets an increasing need to have efficient and accurate numerical tools for modelling complex phenomena, such as pollutant formation during combustion.

Keywords Flow, Fluid dynamics, Simulation

Paper type Research paper

1. Introduction and motivation

Accurate modeling of reactive flows requires the solution of a large number of conservation equations as dictated by detailed reaction mechanism. In addition to the sometimes prohibitively large number of variables introduced, the numerical solution of the governing equations has to face the stiffness due to the fast time scales of the kinetic terms (processes occurring on a wide range of scales ranging from seconds

International Journal of Numerical Methods for Heat & Fluid Flow
Vol. 21 No. 5, 2011
pp. 494-517

0961-5539
DOI 10.1108/09615531111135792

down to nanoseconds). In fact, chemistry acts on top of transport phenomena, whose time scales are typically of the order of millisecond down to microsecond. Those issues make computations of flames, where detailed chemistry is to be accounted, in 2D- and 3D flows extremely time consuming, and have particularly negative impact on the lattice Boltzmann method (LBM), whose number of fields (distribution functions or populations) is significantly larger than the number of fields in conventional methods (density, momenta, temperature, species mass fractions) by a factor ranging from tens to hundreds for 2D and 3D simulations. Moreover, stiffness drastically affects the implementation of explicit numerical solvers (such as the LBM), where reducing the time step becomes compulsory in order to both avoid numerical instabilities and keep a satisfactory accuracy. As a matter of fact, the smallest time scale need to be resolved (with a dramatic increase of the computational time) even if we are only interested in the slow dynamics of the system. Finally, the larger the number of elementary reactions in a detailed combustion mechanism, the more intense the computational effort to evaluate the reaction rates, which typically involves the computation of demanding functions (e.g. exponential functions).

For these reasons, techniques capable of reducing the computational time and the memory demand are particularly desirable in the context of the LBM when simulating reactive flows. In this respect, some reduction might be achieved without a big effort, e.g. by eliminating unimportant reaction steps (or species) from the detailed combustion mechanism. Several tools have been devised to that aim, such as the sensitivity analysis (Rabitz 1987), the comparative analysis of entropy production (Bykov *et al.* 1977; Dimitrov 1977), and the reaction path analysis (Frouzakis and Boulouchos 2000). Nevertheless, the above methodologies are never fully automated, and they often produce results with unsatisfactory accuracy. In the following, we make use of a model reduction technique, the method of invariant grid (MIG) (Gorban *et al.* 2004), based on the notions of time-scale separation and low dimensional manifolds, which present the advantage of an automated implementation (Chiavazzo 2009) and it is expected to recover the asymptotic behavior of the detailed system, with remarkable accuracy (Gorban and Karlin 2005; Chiavazzo *et al.* 2009). In fact, we are often interested in the system behavior on the scale of fluid mechanics (slow dynamics), thus some chemical phenomena (fast dynamics) can be considered self-equilibrated. The general idea behind MIG stems from the geometric picture of relaxation of solution trajectories in the phase-space, and is briefly described below. Dynamics of complex reactive system is often characterized by a short initial transient during which the fast processes evolve and equilibrate, such that the solution trajectory approaches low-dimensional manifolds in the concentration space, known as the slow invariant manifolds (SIMs). The remaining dynamics lasts much longer and evolves along the SIM towards the steady state (see also the Section 2 and Figure 2). Decoupling the fast-equilibrated processes from the slower dynamics does indeed bring a reduction of degrees of freedom into the problem, and can be implemented in a systematic manner by devising effective techniques for constructing SIM in the solution space of the detailed system.

The notion of low-dimensional manifold of slow motions has proved fruitful in model reduction, and it has been widely investigated in chemical kinetics for analyzing and simplifying complex reaction mechanisms. Besides, the already-mentioned MIG by Gorban and Karlin, the most popular methods based on the above concept are,

among others: the computational singular perturbation method by Lam and Goussis (1994), the intrinsic low dimensional manifold (ILDM) by Maas and Pope (Maas and Pope 1992), the invariant constrained equilibrium edge preimage curve method (ICE-PIC) by Ren *et al.* (2006), and the method of minimal entropy production trajectories by Lebiedz (2004).

This work is organized in sections as follows. In Section 2, the kinetic equations describing reactive mixtures are reviewed, and the case of a batch reactor under fixed enthalpy and pressure discussed in more detail. The LB model for reactive flow simulation, adopted in the following, and the hypotheses behind it are reviewed in Section 3. Some basics about the MIG technique are discussed in Section 4. In particular, the notions of quasi-equilibrium manifold film equation and thermodynamic projector are reviewed in Sections 1 and 2, while their application to a bath reactor is reported in Section 3. The coupling between the MIG and the LB model is studied in Section 5, and applied to a 2D laminar flame in Sections 2 and 3. In Section 6, the limits of validity of the presented methodology are discussed, and possible extensions outlined. In Section 7 conclusions are drawn.

2. Gas mixtures in a batch reactor

Below, we focus on mixtures of ideal gases, where n chemical species $x_1, \ldots, x_n$ are involved in a complex reaction consisting of r reversible elementary steps as follows:

$$\nu'_{s1}x_1 + \cdots + \nu'_{sn}x_n \rightleftarrows \nu''_{s1}x_1 + \cdots + \nu''_{sn}x_n, \quad s = 1, \ldots, r, \tag{1}$$

with ν'_{si} and ν''_{si} the stoichiometric coefficient of species i in the reaction step s in the forward and reverse direction, respectively. The reaction rate due to step s takes the expression:

$$\Omega_s = k_s^f \prod_{j=1}^{n} [X_j]\, \nu'_{js} - k_s^r \prod_{j=1}^{n} [X_j]\, \nu''_{js}, \quad s = 1, \ldots, r, \tag{2}$$

where $[X_j]$ denotes the molar concentration of species j. The rate of production (or consumption) of species i in reaction s reads:

$$\dot{\omega}_{is} = \left(\nu''_{is} - \nu'_{is}\right)\Omega_s. \tag{3}$$

Both the forward and reverse reaction rate constants k_s^f and k_s^r are typically expressed using the popular semi-empirical modified Arrhenius formula:

$$k_s(T) = A_s T^{\beta_s} \exp\left(\frac{-E_{as}}{\mathcal{R}T}\right), \tag{4}$$

where A_s is a pre-exponential factor, β_s the temperature exponent, E_s the activation energy of step s and $\mathcal{R}$ the universal gas constant. The total production (or consumption) rate of species i reads:

$$\dot{\omega}_i = \sum_{s=1}^{r} \dot{\omega}_{is}, \tag{5}$$

with the forward and reverse reaction rate constants related by the equilibrium constant $K_{c,s} = k_s^f / k_s^r$, which is obtained imposing the principle of detail balance at the steady state:

$$k_s^f \prod_{j=1}^{n} [X_j]\, \nu'_{js} = k_s^r \prod_{j=1}^{n} [X_j]\, \nu''_{js}, \quad s = 1, \ldots, r. \tag{6}$$

In batch reactors, the gas mixture is a closed system with no mass flux through the boundary, and the state $\psi = (Y_1, \ldots, Y_n)$ evolves in time according to:

$$\mathrm{f} = \left(\frac{dY_1}{dt}, \ldots, \frac{dY_n}{dt} \right) = \left(\frac{\dot{\omega}_1 W_1}{\bar{\rho}}, \ldots, \frac{\dot{\omega}_n W_n}{\bar{\rho}} \right), \tag{7}$$

where Y_i and W_i are the mass fraction and the molecular weight of species i, respectively, while $\bar{\rho}$ represents the mixture mean density. In order to close the kinetic equation system (7), an additional condition for the temperature dynamics is required. In the following, we refer to closed isoenthalpic isobaric systems where the equation for temperature stipulates the constance of the mixture averaged enthalpy $\bar{h}$:

$$\bar{h} = \sum_{i=1}^{n} h_i(T) Y_i = const, \tag{8}$$

where h_i denotes the enthalpy of species i, whose temperature dependence is accounted using a polynomial fit:

$$h_i(T) = R\left(a_{1i} T + \frac{a_{2i}}{2} T^2 + \frac{a_{3i}}{3} T^3 + \frac{a_{4i}}{4} T^4 + \frac{a_{5i}}{5} T^5 + a_{6i} \right), \tag{9}$$

expressed in terms of the NASA coefficients a_{ij}, tabulated for each species i, with $j = 1, \ldots, 7$. More specifically, the temperature dynamics obeys the following equation:

$$\bar{c}_p \frac{dT}{dt} = -\frac{1}{\bar{\rho}} \sum_{i=1}^{n} h_i \dot{\omega}_i W_i. \tag{10}$$

Finally, in a closed reactor, the atom mole numbers N_k of each element k is conserved:

$$D\psi T = (N_1, \ldots, N_d)^T, \quad \frac{dN_k}{dt} = 0, \quad D(k,i) = \frac{\mu_{ik}}{W_i}. \tag{11}$$

Here, μ_{ik} is the number of atoms of the kth element in species i, and D is a $(d \times n)$ matrix, where d is the number of elements involved the reaction. In other words, the vector field f in equation (7) remains always orthogonal (in the Euclidean sense) to the raws of D.

3. Model for reactive flow simulations

In the present work, for the sake of simplicity, we apply the following assumptions to the governing equations for reactive flows in the low Mach number regime:

- The flow field is assumed incompressible and it is not affected by the chemical reaction.
- The transport properties are constant.

- The Fick's law applies to diffusion.
- Viscous energy dissipation and radiative heat transfer can be neglected.

It is worth noticing that we make use of the above simplifications, since they are not essential to the issues of model reduction for reactive flows simulations, which is our major concern here. In fact, the suggested methodology can be applied also when all the above hypothesis are relaxed. In such a framework, the velocity field u_i and pressure p can be described by solving the mass and momentum conservation equations as dictated by the incompressible Navier-Stokes formulation (in the absence of body forces):

$$\partial_j u_j = 0, \quad \partial_t u_i + u_j \partial_j u_i = -\frac{1}{\bar{\rho}} \partial_i p + \partial_j (\nu \partial_j u_i), \tag{12}$$

where ∂_t, ∂_j, ν and $\bar{\rho}$ denote partial derivatives with respect to time, partial derivatives with respect to the jth spatial direction, the kinematic viscosity and the mixture density, respectively, while Einstein summation convention is assumed for the repeated indexes. Moreover, the governing equations of the mixture-averaged enthalpy $\bar{h}$ and the mass fraction Y_i of the ith chemical species has to be taken into account as follows:

$$\partial_t \bar{h} + u_j \partial_j \bar{h} = \partial_j \left(\kappa \partial_j \bar{h} \right) + \sum_{i=1}^{n} \frac{\dot{\omega}_i W_i}{\bar{\rho}} h_i, \tag{13}$$

$$\bar{\rho} \left(\partial_t Y_i + u_j \partial_j Y_i \right) = \partial_j \left(\bar{\rho} D_i \partial_j Y_i \right) + \dot{\omega}_i W_i, \tag{14}$$

where κ and D_i are the thermal diffusivity and the diffusion coefficient of species i, respectively.

3.1 LBM for combustion

Here, we consider the simple LB formulation suitable for combustion field computations suggested in Yamamoto *et al.* (2002), whereas more elaborate LB models for mixtures (Arcidiacono *et al.*, 2007; Asinari, 2009) and compressible flows (Prasianakis and Karlin, 2007) shall be investigated in the near future, too. It has been proven that model in Yamamoto *et al.* (2002) is able to describe reactive flows consistently with the continuum approach where the equations (12)-(14) are used.

The LBM is a relatively novel approach to numerical flow simulations, and it can be regarded as a special discretization of the Boltzmann equation which is known to be the governing equation of gas dynamics (Succi, 2001). This method consists of discrete and explicit kinetic equations expressed in terms of a small set of particles distribution functions (populations for short). Those kinetic equations are designed in such a way that the continuum description (Navier-Stokes equations) is recovered in the hydrodynamic limit, where the Knudsen number is small. Each population moves on a regular lattice at a different velocity: in Figure 1, we show a popular scheme for 2D simulations, where nine populations are represented by their own peculiar velocity e_α.

In the following, the flow field is treated as a single-component medium that can be described, in terms of pressure distribution functions p_α, by the following equation at an arbitrary lattice node x (Succi, 2001):

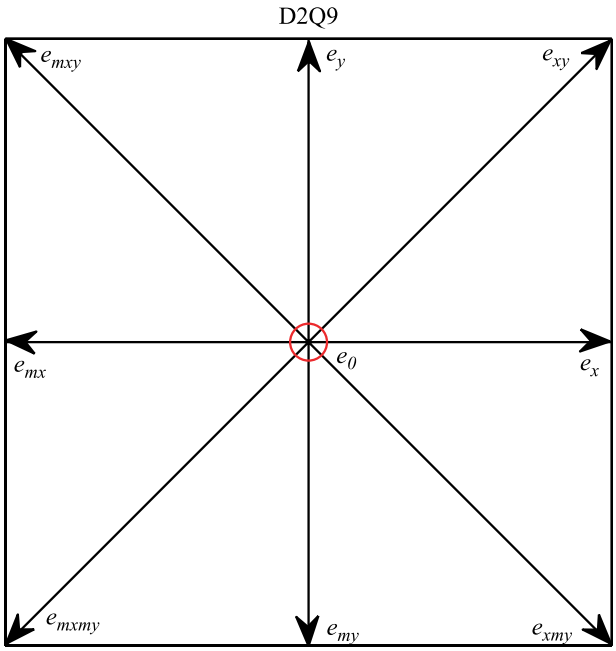

Figure 1.
Two-dimensional nine-velocity stencil: D2Q9

$$p_\alpha(x + e_\alpha, t + \delta t) = p_\alpha(x,t) - \frac{1}{\tau_F}\left[p_\alpha(x,t) - p_\alpha^{eq}(p,u)\right], \tag{15}$$

where the equilibrium populations p_α^{eq} read:

$$p_\alpha^{eq} = w_\alpha p\left[1 + 3\left(e_\alpha u^T\right) + \frac{9}{2}\left(e_\alpha u^T\right) - \frac{3}{2}u^2\right]. \tag{16}$$

The pressure p and the fluid velocity u are given by:

$$p = \sum_\alpha p_\alpha, \quad u = \frac{1}{p_0}\sum_\alpha e_\alpha p_\alpha, \tag{17}$$

where the reference pressure $p_0 = \rho_0/3$, with ρ_0 denoting the reference density of the LB model. Let δt be the time step, the relaxation parameter τ_F can be linked to the kinematic viscosity ν, e.g. by performing an asymptotic analysis of the LB equation (Chapman and Cowling, 1970; Chen and Doolen, 1998):

$$\nu = \frac{2\tau_F - 1}{6}\,\delta t. \tag{18}$$

In general, the discrete velocities can be regarded as the nodes of a Gauss-Hermite quadrature applied to the Maxwell-Boltzmann distribution function, and each of them is characterized by a proper weight w_α (Succi, 2001; Karlin *et al.*, 1999). According to Yamamoto *et al.* (2002), the flow field is not affected by the chemical reaction, transport coefficients are constant and Fick's law applies to the diffusion. Let $\bar{h}_0$ be a reference enthalpy, the evolution equations for enthalpy and concentration of species i are written as:

$$\tilde{h}\alpha(x+e_\alpha,t+\delta t)-\tilde{h}_\alpha(x,t)=-\frac{1}{\tau_h}\left[\tilde{h}_\alpha(x,t)-\tilde{h}_\alpha^{eq}(\tilde{h},u)\right]+w_\alpha Q_h, \tag{19}$$

$$Y_{i\alpha}(x+e_\alpha,t+\delta t)-Y_{i\alpha}(x,t)=-\frac{1}{\tau_{Y_i}}\left[Y_{i\alpha}(x,t)-Y_{i\alpha}^{eq}(Y_i,u)\right]+w_\alpha Q_{Y_i}, \tag{20}$$

where:

$$\tilde{h}=\frac{\bar{h}}{\bar{h}_0}=\sum_\alpha \tilde{h}_\alpha,\quad Y_i=\sum_\alpha Y_{i\alpha}, \tag{21}$$

and the equilibrium populations $\tilde{h}_\alpha^{eq}$, $Y_{i\alpha}^{eq}$ are expressed as in equation (16) after replacing p with $\tilde{h}$ and Y_i, respectively. Assume t_0 is a factor for converting physical time into LB time units: $(t)_{LB}=(t)_{phys}/t_0$, the source terms take the explicit form:

$$Q_h=\frac{1}{h_0}\left(\sum_{i=1}^{9}\frac{\dot{\omega}_i W_i}{\bar{\rho}}\,h_i\right)t_0\delta t, Q_{Y_i}=\frac{\dot{\omega}_i W_i}{\bar{\rho}}\,t_0\delta t, \tag{22}$$

where $\bar{\rho}$ is the mixture-averaged density, while $\dot{\omega}_i$, W_i, h_i denote the rate of change, molecular weight and enthalpy of species i, respectively. Similarly to the kinematic viscosity, the thermal diffusivity κ and diffusion coefficient D_i of species i are related to the relaxation parameters as follows:

$$\kappa=\frac{2\tau_h-1}{6}\,\delta t,\quad D_i=\frac{2\tau_{Y_i}-1}{6}\,\delta t. \tag{23}$$

4. Model reduction technique

In our study, the reduced model is obtained using the MIG. The detailed mechanism of Li *et al.* (2004) (nine species, 21 elementary reactions) for hydrogen combustion is considered, and our goal is to search for a reduced description with only a few degrees of freedom. In particular, here we are interested in a reduced description, where the combustion mechanism is governed by two chemical coordinates. Below, a general overview of MIG method is given, while more details can be found in the literature (Gorban and Karlin, 2005; Gorban *et al.*, 2004; Chiavazzo and Karlin, 2008; Chiavazzo *et al.*, 2007, 2009).

4.1 MIG initialization

For our purposes, the MIG technique can be initially applied to a spatially homogeneous reactor under constant mixture-averaged enthalpy and pressure at a fixed equivalence ratio ϕ. To this end, we first construct a 2D QEM for a stoichiometric H_2-air mixture under fixed pressure p and enthalpy $\bar{h}$. In general, a q-dimensional QEM is obtained solving the following minimization problem:

$$\begin{cases} G\rightarrow min \\ \sum_i m_j^i Y_i=\xi^j, \quad j=1,\ldots,q, \end{cases} \tag{24}$$

where G is a thermodynamic Lyapunov function with respect to the kinetic equation (7). It is well known from thermodynamics that, in a closed reactive system under fixed enthalpy and pressure, the latter function is given by the mixture-averaged entropy. Moreover, the vector set $\{\mathrm{m}_j = (m_j^1, \ldots, m_j^9)\}$ is adopted in order to re-parameterize the primitive variables Y_i (mass fraction) in terms of new lumped quantities ξ^j, whose dynamics is expected to be slower than Y_i. QEMs attempt a fast-slow motion decomposition of the kinetic system dynamics, where the slow movements are assumed to occur (throughout the entire composition space) in the subspace spanned by the vectors m_j, while fast motions occur in its orthogonal complement. The notion of QEM can provide with an approximated reduced description in chemical kinetics at a reasonable computational cost, hence it has been widely exploited for that purpose (Tang and Pope, 2004; Hamiroune *et al.*, 1998; Chiavazzo and Karlin, 2008). Several suggestions for defining slow-lumped variables in chemical kinetics are known from the literature. In that respect, it is worth mentioning here the parameterization utilized in the rate controlled constrained equilibrium (RCCE) method (Keck and Gillespie, 1971), where a physical meaning is directly attached to the slow parameters ξ. For instance, in the case of hydrogen combustion, the following quantities:

$$\begin{aligned}
\xi^1 &= \sum_i \frac{Y_i}{W_i}, \\
\xi^2 &= \frac{Y_O}{W_O} + \frac{Y_{OH}}{W_{OH}} + \frac{Y_{H_2O}}{W_{H_2O}}, \\
\xi^3 &= \frac{Y_H}{W_H} + 2\frac{Y_O}{W_O} + \frac{Y_{OH}}{W_{OH}},
\end{aligned} \tag{25}$$

related to the total number of moles, the number of moles of free oxygen and the active valence, respectively, may be adopted for constructing up to 3D QEMs (Tang and Pope, 2004). Moreover, a more systematic parameterization of a QEM has been introduced recently Chiavazzo *et al.* (2007), where the vectors m_j are defined on the basis of the left eigenvectors of the Jacobian matrix:

$$\mathrm{J} = \begin{bmatrix} \frac{\partial f_1}{\partial Y_1} & \cdots & \frac{\partial f_1}{\partial Y_n} \\ \vdots & \ddots & \vdots \\ \frac{\partial f_n}{\partial Y_1} & \cdots & \frac{\partial f_n}{\partial Y_n} \end{bmatrix}, \tag{26}$$

computed at the steady state: spectral QEM. Here, f_i is the ith component of the vector field (7). Notice that, in the following, we always deal with a discrete representation of a manifold (grid), namely sets of states (points in the concentration space) and connections between them that allow us to define the grid tangent space at each node (see also Section 2).

An approximated solution to equation (24), called quasi equilibrium grid (QEG), can be computed making use of the algorithm introduced in Chiavazzo and Karlin (2008) and briefly reviewed below. According to the latter algorithm, an initial grid is

constructed starting from a known state (seed) of the QEM (typically the steady state) upon linearization of the problem (24). Therefore, extension of a grid along the kth parameter ξ^k is accomplished by solving the linear system:

$$\begin{aligned}
&\sum_{i=1}^{z} \left(\mathrm{t}_j \boldsymbol{H} \boldsymbol{\rho}_i^T\right) \varphi_i = -t_j \nabla G^T, \quad j = 1, \ldots, z-q \\
&\sum_{i=1}^{z} \left(\boldsymbol{m}_1 \boldsymbol{\rho}_i^T\right) \varphi_i = 0, \\
&\qquad \vdots \\
&\sum_{i=1}^{z} \left(\boldsymbol{m}_k \boldsymbol{\rho}_i^T\right) \varphi_i = \varepsilon_k, \\
&\qquad \vdots \\
&\sum_{i=1}^{z} \left(\boldsymbol{m}_q \boldsymbol{\rho}_i^T\right) \varphi_i = 0,
\end{aligned} \tag{27}$$

with respect to the unknowns φ_i, where ∇G and $\boldsymbol{H}$ signify the gradient and the second derivative matrix of G, respectively, computed at the seed, under constant mixture enthalpy $\bar{h}$ and pressure p. Let E be a matrix obtained by adding the parameterization vectors m_j as additional rows to the matrix of atom conservations D defined in equation (11), the two vector bases $\{\rho_1, \ldots, \rho_z\}$ and $\{t_1, \ldots, t_{z-q}\}$ span the null space of D and E, respectively:

$$\boldsymbol{D} = \begin{bmatrix} \frac{\mu_{11}}{W_1} & \cdots & \frac{\mu_{n1}}{W_n} \\ \vdots & \ddots & \vdots \\ \frac{\mu_{1d}}{W_1} & \cdots & \frac{\mu_{nd}}{W_n} \end{bmatrix}, \quad \boldsymbol{E} = \begin{bmatrix} & \boldsymbol{D} & \\ m_1^1 & \cdots & m_1^n \\ \vdots & \ddots & \vdots \\ m_q^1 & \cdots & m_q^n \end{bmatrix}, \tag{28}$$

with $z = n - d$ denoting the dimension of the null space of the matrix $\boldsymbol{D}$. Let $\mathrm{c}^0 = (c_1^0, \ldots, c_n^0)$ be the seed, the new QE-grid state c^1, in a neighborhood of c^0, has the following coordinates $\mathrm{c}^1 = (c_1^0 + dc_1^0, \ldots, c_n^0 + dc_n^0)$, with:

$$(dc_1^0, \ldots, dc_n^0) = \sum_{i=1}^{z} \varphi_i \rho_i.$$

When dealing with isobaric isenthalpic systems, G is related to the mixture averaged entropy $\bar{s}$ which, for ideal gas mixtures, takes the following explicit form:

$$G_{p,\bar{h}} = -\bar{s} = -\frac{1}{\bar{W}} \sum_{i=1}^{n} \left[s_i(T) - \mathcal{R} \ln(X_i) - \mathcal{R} \ln\left(\frac{p}{p_{ref}}\right) \right] X_i, \tag{29}$$

where $\bar{W}$, $\mathcal{R}$, X_i, p and p_{ref} denote the mean molecular weight, the universal gas constant, the mole fraction of species i, the total pressure and a reference pressure, respectively. The specific entropy s_i is assumed to have the following dependence on the temperature T:

$$s_i(T) = \mathcal{R}\left(a_{i1}\ln T + a_{i2}T + \frac{a_{i3}}{2}\,T^2 + \frac{a_{i4}}{3}\,T^3 + \frac{a_{i5}}{4}\,T^4 + a_{i7}\right) \tag{30}$$

where, for each chemical species i, a_{ij} are given by the NASA coefficients.

In the following, in order to save notation, it proves convenient to define both the following entropic scalar product between two arbitrary vectors $\boldsymbol{x}$ and $\boldsymbol{y}$:

$$\langle \boldsymbol{x}, \boldsymbol{y} \rangle = \boldsymbol{x}\boldsymbol{H}\boldsymbol{y}^T, \tag{31}$$

and the functional:

$$DG(x) = \nabla G \boldsymbol{x}^T \tag{32}$$

where the superscript T signifies transposition.

Finally, notice that computing first and second derivative of G is not straightforward, since equation (29) explicitly depends on the mixture temperature T, which is in turn implicit function of the enthalpy $\bar{h}$ as dictated by the non-linear relation (9). However, to this end, both approximate, e.g. finite differencing (FD), and exact approaches, e.g. automatic differentiation (AD), can be adopted. According to FD, the exact first derivative is approximated by the following ratio:

$$\left.\frac{\partial G}{\partial Y_i}\right|_{p,\bar{h}} \simeq \frac{G\left(T', \ldots, Y_i + \varepsilon, \ldots\right) - G\left(T', \ldots, Y_i, \ldots\right)}{\varepsilon}, \tag{33}$$

where ε is a small parameter, while the temperature T' satisfies the following equation:

$$\bar{h}\left(T', \ldots, Y_i + \varepsilon, \ldots\right) = \bar{h}\left(T', \ldots, Y_i, \ldots\right). \tag{34}$$

Typically, in order to achieve the best accuracy and minimize the round-off error, ε is chosen of the order of the square root of the machine precision. Moreover, forward (or backward) finite difference schemes are preferred for first derivatives, and central schemes are adopted for second derivatives. On the other hand, AD enables to differentiate (in principle up to any order) the subroutine itself that computes the function (29), by systematically applying chain rule to the entire sequence of elementary assignments of the code. Although AD can be significantly slower than FD (up to an order of magnitude), it provides with exact values of the derivatives. Alternatively, the explicit and exact formulas reported in Chiavazzo (2009) can be adopted.

4.2 MIG refinements

In general, by the term *manifold*, it is meant a q-dimensional surface Ω embedded in the n-dimensional phase space, and defined my the mapping in a parameter space Ξ into the phase space U: $\psi = F\left(\xi^1, \ldots, \xi^q\right)$, with ψ denoting an arbitrary state of U. A consistent way of model reduction is to construct a positively invariant slow manifold Ω_{inv} (with respect to the kinetic system (7)) such that the vector field $\boldsymbol{f}$ is tangent to Ω_{inv} at any point of it (Gorban and Karlin, 2005). On the other hand, towards the end of a discrete representation of manifolds, grids $\mathcal{G}$ are introduced as independent objects (Gorban *et al.*, 2004), and defined by a mapping $F\left(\xi^1, \ldots, \xi^q\right)$ of a finite subset of the parameter space Ξ into the phase space of the system (7). Hence, invariant grids consist of a discrete set of nodes, where each of them can be represented by a vector of species mass fractions. Moreover, connectivity between the nodes is

utilized in order to introduce differentiation operators, calculate the tangent vectors and define the projector operator as defined below in this section.

It is worth stressing that the choice of the vector set $\boldsymbol{m}_j$ has a significant influence on the accuracy of the corresponding QEM in describing the SIM (Chiavazzo *et al.*, 2007). Nevertheless, the above construction only represents the first step of the MIG technique, given that a QE-grid $\mathcal{G}$ has to be anyway refined as described below in this section. The refined grid (invariant grid) is an accurate discrete approximation of the SIM, hence it does not depend on the chosen parameterization.

Let a unique mapping $\psi = F(\xi^1, \ldots, \xi^q)$ define a grid $\mathcal{G}$. Let a reconstruction procedure (e.g. polynomial interpolation) be chosen, such that derivatives $\partial F/\partial \xi^i$ can be computed and the local tangent space to $\mathcal{G}$ defined.

According to MIG, the invariant grid of the kinetic system can be computed by relaxation of $\mathcal{G}$ under the following film equation of dynamics (Gorban and Karlin 2005):

$$\frac{d\mathcal{G}}{dt} = \boldsymbol{f} - \boldsymbol{P}\boldsymbol{f}, \tag{35}$$

where $\boldsymbol{f}$ and $\boldsymbol{P}$ denote the vector of motion in the phase space and a projector operator onto the grid tangent space, respectively. In general, the operator $\boldsymbol{P}$ can be any matrix which satisfies the condition $\boldsymbol{P}^2 = \boldsymbol{P}$, such that the vector $\boldsymbol{P}\boldsymbol{f}$ belongs to the tangent space. Here, however, we adopt the thermodynamic projector (Gorban and Karlin, 1992), which enables to identify the fast motions toward the slow manifolds.

The thermodynamic projector is based on the following idea: if a given manifold indeed represents the manifold of slow motions, then the Lyapunov function G has been increasing during the fast process of relaxation towards this manifold. Therefore, the points of the manifold appear as the minimum points of the Lypunov function on the manifolds of fast motion. The latter can be approximated accurately in a small vicinity of the slow manifold using the Lyapunov function gradient at the points of SIM. The thermodynamic projector $\boldsymbol{P}$ in fact formalizes this intuitive picture as reported below. Importantly, $\boldsymbol{P}$ is updated on each iterations when seeking the SIM from the film equation.

Let the derivatives $\partial F/\partial \xi^i$ define the tangent space T_ψ, at each grid point ψ:

$$T_\psi = Lin\left\{\frac{\partial \xi^i}{\partial F}\right\}, \quad i = 1, \ldots, q. \tag{36}$$

The subspace $T_{\psi,0} = (T_\psi \cap \ker DG)$ defines, if $T_\psi \neq T_{\psi,0}$, the tangent vector $e \in T_\psi$, through the following conditions:

$$DG(\boldsymbol{e}) = 1, \quad \langle \boldsymbol{e}, \boldsymbol{x} \rangle = 0, \quad \forall \boldsymbol{x} \in T_{\psi,0}, \tag{37}$$

so that, the thermodynamic projection of an arbitrary vector $\boldsymbol{x}$ has the form:

$$\boldsymbol{P}\boldsymbol{x} = DG(x)e + \sum_{i=1}^{q-1} \langle \boldsymbol{k}_i, \boldsymbol{x} \rangle \boldsymbol{k}_i. \tag{38}$$

The basis $\{\kappa_1, \ldots, \kappa_{q-1}\}$ (orthonormal with respect to the entropic scalar product (31)) spans the subspace $T_{\psi,0}$. In the case $T_\psi \equiv T_{\psi,0}$, the projector (38) becomes:

$$\boldsymbol{Px} = \sum_{i=1}^{q} \langle \boldsymbol{\kappa_i}, \boldsymbol{x} \rangle \boldsymbol{\kappa_i}. \tag{39}$$

Here, it is worth stressing the relevant feature of the latter projector. Let us consider a q-dimensional SIM in a n-dimensional phase space. The above construction is based on the idea that the thermodynamic considerations (minimization of the thermodynamic Lyapunov function) are solely required to construct fast manifolds in the vicinity of SIM. On the other hand, if it is possible to describe the fast subspace in different terms (for example, as a result of a different algorithm for construction of SIM), both representations of fast motions should be consistent. Let a vector $a_{r_i}(\psi)$ be a generic vector of the fast subspace. Then:

$$a_{r_i}(\psi) \in \ker P, \quad \forall i = 1, \ldots, n - q, \tag{40}$$

where $\ker P$ is the null space of equation (38) evaluated at ψ. In other words, the thermodynamic projection of fast directions, in a neighborhood of the SIM vanishes.

Finally, as an example, a 2D QEG of a reactive H_2-air mixture with $\bar{h} = 600 >$ kJ/kg, $p = 2$ bar and $\phi = 1$ is constructed as illustrated in the Section 1 above, making use of the spectralquasi equilibrium parameterization. The refined grid is shown in Figure 2, where typical solution trajectories attracted to the grid and relaxing towards the steady state are also reported.

4.3 Integration of the reduced system

Once a q-dimensional invariant grid is constructed (typically with $q \ll n$), the set of kinetic equations (7) (problem with $(n - d)$ degrees of freedom) admits a reduced description with q degrees of freedom. In fact, the system dynamics along invariant grids:

$$\left(\frac{dY_1}{dt}, \ldots, \frac{dY_n}{dt}\right) sT = \boldsymbol{Pf}, \tag{41}$$

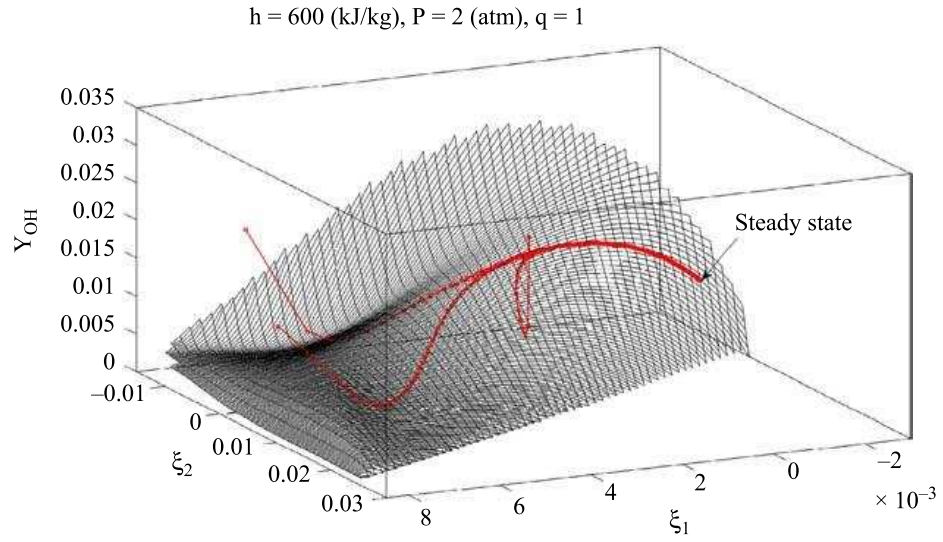

Notes: Example of a 2D invariant grid (black continuous lines); samples of solutions trajectories (circles) relaxing towards the invariant two-dimensional grid are reported

Figure 2.
Batch reactor under constant enthalpy and pressure at stoichiometric proportions

can be recast in a smaller set of differential equations, by recalling the definition of the parameters ξ^i:

$$\left(\frac{d\xi^1}{dt}, \ldots, \frac{d\xi^q}{dt}\right) = \left(\mathrm{m}_1 \boldsymbol{Pf}, \ldots, \mathrm{m}_q \boldsymbol{Pf}\right). \tag{42}$$

Notice that, the projector $\boldsymbol{P}$ of the reduced systems (41) and (42) must be constructed as prescribed in Section 2. Indeed, in this case, the fast directions belong to the null space of the thermodynamic projector, and the right-hand side of equations (41) and (42) is characterized by a reduced stiffness with respect to the original system (7) (Chiavazzo *et al.* 2010). The right-hand side of equation (42) can be tabulated along with the node coordinates and the parameters ξ^j, before solving the reduced system. However, a reconstruction procedure, such as a multi-variate interpolation, is typically adopted in order to evaluate the rates equation (42) at an arbitrary point of the phase-space.

Using the 2D invariant grid shown in Figure 2, we report a comparison between the solution of the detailed kinetic model (7) and the reduced one equation (42), starting from an arbitrary initial condition of the grid (Figures 3 and 4). Excellent agreement between the two descriptions can be observed, whereas the time step used in the numerical solver (explicit fourth order Runge-Kutta) of the reduced model can be chosen an order of magnitude larger than the one for the detailed one, due to the reduced stiffness of equation (42).

Remark. For the sake of completeness, we highlight here some relevant differences between the MIG methodology and other model reduction methods based on the notion

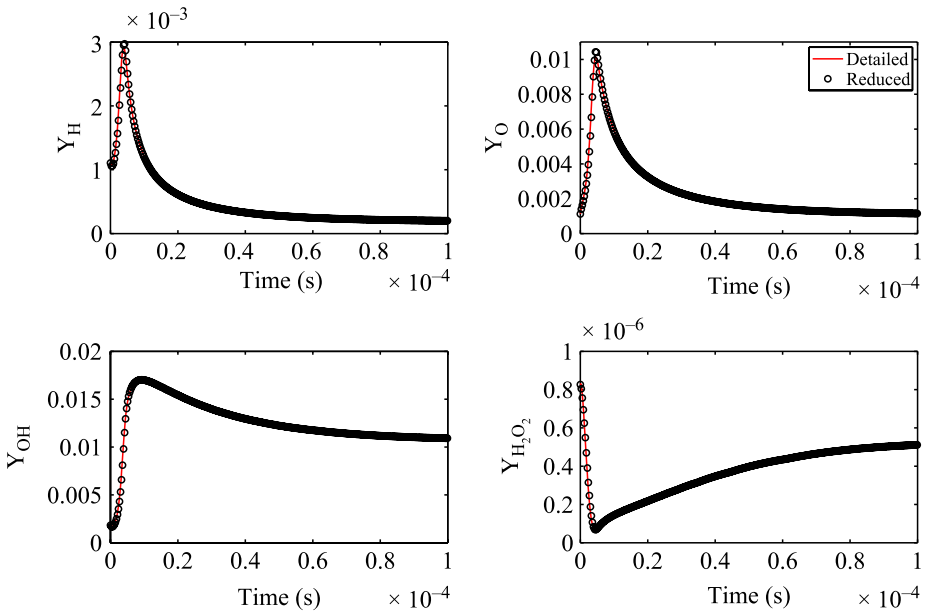

Figure 3.
Batch reactor under constant enthalpy and pressure at stoichiometric proportions

Notes: Specie mass fraction dynamics, as dictated by the detailed model (continuous lines), is compared to the corresponding reduced model solution, where the initial condition belongs to a 2D invariant grid; problems with an initial condition not on the 2D invariant grid can be similarly addressed, on the basis of the thermodynamic projector (38), as discussed in Chiavazzo *et al.* (2010)

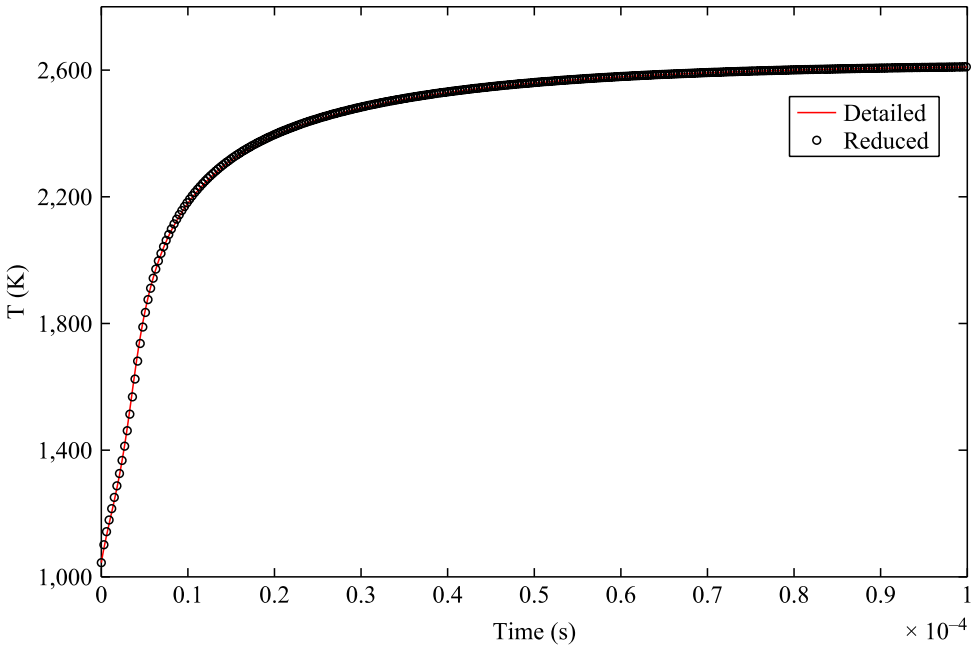

Notes: Temperature dynamics, as dictated by the detailed model (continuous lines), is compared to the corresponding reduced model solution, where the initial condition belongs to a 2D invariant grid; problems with an initial condition not on the 2D invariant grid can be similarly addressed, on the basis of the thermodynamic projector (38), as discussed in Chiavazzo *et al.* (2010)

Figure 4.
Batch reactor under constant enthalpy and pressure at stoichiometric proportions

of low-dimensional manifolds. According to the method of invariant manifolds (MIM) (Gorban and Karlin, 2005), and its discrete formulation (MIG), the problem of description reduction of a detailed model is identified with the construction of a SIM Ω_{inv} embedded in the phase space U, and represented by a function F mapping a parameter space Ξ into U. Introducing a projector P onto the tangent space of a manifold, invariance can be imposed relatively straightforwardly by seeking for the stationary point of the film equation (35):

$$\boldsymbol{f}(F) - \boldsymbol{P}\boldsymbol{f}(F) = 0. \tag{43}$$

However, a definition of slowness, which necessarily compares a (faster) approach towards the SIM with (slower) motions along SIM, is more delicate: in MIM (and MIG) slow-fast motion separation is unambiguously defined on the basis of the thermodynamic projector (38), as described in Section 2, and this is a peculiar feature of the latter technique. On the other hand, in other methods such as the ILDM method (Maas and Pope, 1992) slow and fast subspaces are computed (approximately) by spectral decomposition of the Jacobian matrix (26): As a result, in general, the constructed ILDM is not invariant and sometimes ill defined (Borok *et al.*, 2008). Moreover, the QEM and RCCE method (Keck and Gillespie, 1971) are based on a priori assumptions about slow and fast variables of the kinetic system (7), and often provide with unsatisfactory approximated descriptions of the corresponding SIM (Tang and Pope, 2004; Chiavazzo *et al.*, 2007). Therefore, the MIM (and MIG) only regards both the QEM and RCCE as initial approximations of SIM which must be further refined, and it thereby enables to significantly enhance the accuracy of a reduced description. Other approaches (see, e.g. the methods in Ren *et al.* (2006); Roussel and Fraser (1993); Singh *et al.* (2002); Duchene and Rouchon (1996) aim at

constructing invariant manifolds, which thus satisfy the condition (43); however, due to non-uniqueness of its solution (note that, for instance, each solution trajectory of the system (7) is, by a definition, invariant with respect to equation (7)), different methods generally construct different objects. In that respect, as extensively discussed in Chiavazzo *et al.* (2010), in MIG thermodynamics helps in discriminating the invariant manifold of the slow motions (i.e. SIM), and it plays an important role in reducing the stiffness of the system (42).

5. 2D premix laminar flame

In this section, we illustrate the coupling methodology between a reduced model obtained from the MIG procedure, and the LB model for reactive flows reviewed in Section 3. For simplicity, in the following, we use the assumption of equal diffusivity D for all species and Lewis number $Le = \kappa/D = 1$. In this case, the mixture enthalpy $\bar{h}$ and the element fractions remain constant throughout the domain, and the reduced dynamics takes place along a single invariant grid. Notice however that, the latter assumption is not restricting and a generalization is obtained by extending the invariant grid with enthalpy and element fractions as additional degrees of freedom (see also Section 6 below). Moreover, in low-Mach combustion, the pressure p can be considered constant for most cases. Under the latter assumptions, the equation (20) can be written in terms of the slow-manifold parameters ξ^1, ξ^2 as follows:

$$\xi^j_\alpha(\boldsymbol{x} + e_\alpha, t + \delta t) - \xi^j_\alpha(\boldsymbol{x}, t) = -\frac{1}{\tau_\xi}\left[\xi^j_\alpha(\boldsymbol{x}, t) - \xi^{jeq}_\alpha\left(\xi^j, \boldsymbol{u}\right)\right] + w_\alpha Q_{\xi^j}, \tag{44}$$

where, the equilibrium populations for the reduced variables ξ^j read:

$$\xi^{jeq}_\alpha = w_\alpha \xi^j\left[1 + 3\left(e_\alpha \boldsymbol{u}^T\right) + \frac{9}{2}\left(e_\alpha \boldsymbol{u}^T\right) - \frac{3}{2}\boldsymbol{u}^2\right], \tag{45}$$

and the source terms take the form:

$$Q_{\xi^j} = \sum_{i=1}^{9} m^i_j Q_{Y_i}, \xi^j = \sum_{i=1}^{9} m^i_j Y_i. \tag{46}$$

5.1 Example

Here, we consider the 2D laminar burner schematically shown in Figure 5, where several vertical nozzles, ejecting a premixed mixture of hydrogen and air, are put side by side at a fixed distance. A fully premixed hydrogen/air mixture, initially at room temperature (300 K), is ignited by a spark which is simulated by placing a hot spot in a corner of the computational domain. A propagating flame front is thus generated in the flow, while the burned gas exits from the top side of the domain. Because of the geometric symmetry, and under the assumption of laminar flow, the computations can be restricted to a rectangular domain, whose left and right edges are both symmetry axis (Figure 5). In the present configuration, the burner slot is 0.4 mm wide, the nozzle thickness and the domain height are assumed 0.1 mm and 7.31 mm, respectively, while the distance between the centerlines of two contiguous nozzles is 2.84 mm. Note that, each single nozzle can be considered a two-dimensional representation of a Bunsen burner. The flame dynamics might be predicted by solving both the detailed

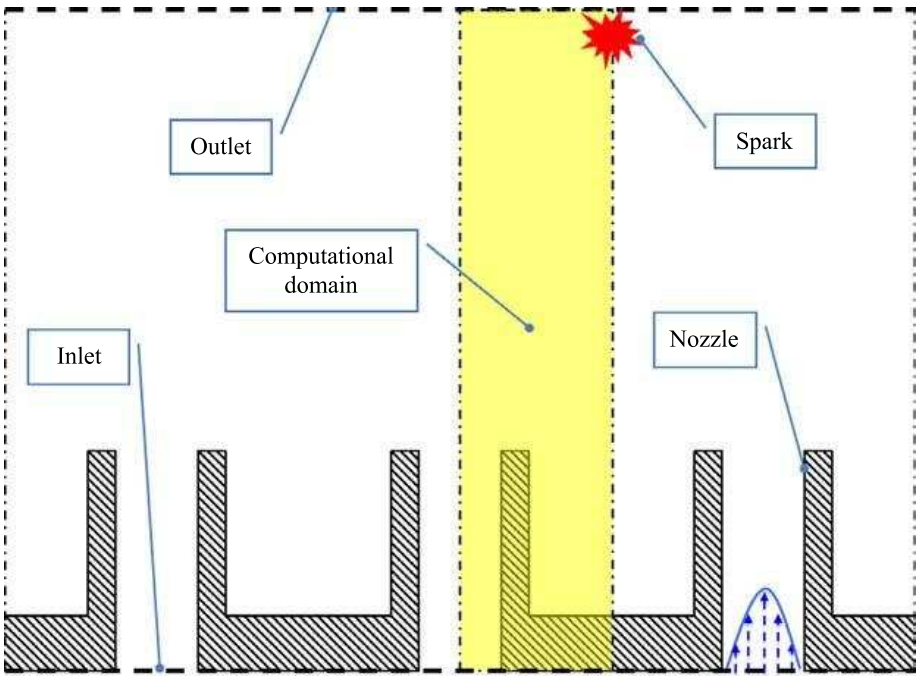

Note: Owing to the symmetric geometry, computations can be restricted to a rectangular domain

Figure 5.
Sketch of a 2D burner

models (19), (20) and the reduced one (44). In the following, we focus on the latter option, where the source terms Q_{ξ^j} are tabulated at each node of the invariant grid, and accessed through multi-variate linear interpolation.

Notice that, all the quantities in LB units are dimensionless, thus transport coefficients and chemical source terms need to be properly converted with the help of analogy. Let L_{phys} and u_{phys} be the height of the computational domain and the norm of flow velocity at the inlet along the symmetry axis in physical units, respectively: (m) and (m/s). Let L_{LB} and u_{LB} be the corresponding dimensionless quantities (LB units). It proves convenient to define the following conversion factors:

$$t_0 = \frac{\left(L_{phys}/u_{phys}\right)}{\left(L_{LB}/u_{LB}\right)}, \quad L_0 = \frac{L_{phys}}{L_{LB}}, \tag{47}$$

such that physical time expressed in (s) and length in (m) can be converted into LB units dividing by t_0 and L_0, respectively. For instance, the diffusion coefficient D_i ([m^2/s]) and the source term $\dot{\omega}_i W_i/\bar{\rho}$ ([s^{-1}]) of species i become in LB units:

$$(D_i)_{LB} = D_i \frac{t_0}{L_0^2}, \quad \left(\frac{\dot{\omega}_i W_i}{\bar{\rho}}\right)_{LB} = \frac{\dot{\omega}_i W_i}{\bar{\rho}}\, t_0. \tag{48}$$

5.2 Flow field computation

In this simulation, we make use of a 65(Nx) × 330(Ny) regular lattice, and impose constant kinematic viscosity: $\nu = 1.5 \times 10^{-5}\,m^2/s$. At the inlet, we impose the equilibrium populations corresponding to pressure $p = 1\,bar$, while the velocity is chosen according to a parabolic profile, with maximum value: $u_{max} = 3.6\,m/s$. Symmetry condition is

imposed using the mirror bounce-back scheme to the missing populations, along the vertical boundaries of the computational domain:

$$\begin{aligned} p_x &= p_{mx}, \quad p_{xy} = p_{mxy}, \quad p_{xmy} = p_{mxmy} \\ p_{mx} &= p_x, \quad p_{mxy} = p_{xy}, \quad p_{mxmy} = p_{xmy} \end{aligned} \tag{49}$$

for the left and right boundary, respectively. At the outlet, fully developed boundary condition is used by zeroth order extrapolation of the second uppermost node:

$$p_\alpha(i, N_y) = p_\alpha(i, N_y - 1), \quad i = 1, \ldots, N_x. \tag{50}$$

Finally, walls are treated imposing the usual bounce back condition: for instance, the inner wall of the nozzle is simulated as follows:

$$p_{mx} = p_x, \quad p_{mxy} = p_{xmy}, \quad p_{mxmy} = p_{xy}. \tag{51}$$

In Figure 6, we report both the streamlines and the magnitude (Euclidean norm) of the velocity field after a large (120,000) number of LB steps.

5.3 Species computation

Dynamics of species mass fraction and temperature field have been computed by means of the equations (44), whereas ξ^1, ξ^2 represent, according to equation (25), the total number of moles and the free oxygen, respectively, and parameterize a two-dimensional invariant grid constructed under fixed enthalpy $\bar{h} = 2.8\,\text{kJ/kg}$ and pressure $p = 1\,\text{bar}$ at stoichiometric proportion (corresponding to the temperature 300 K of the unburned mixture). As illustrated in Section 3 in the case of a homogeneous batch reactor, primitive variables can be afterwards reconstructed via multi-variate interpolation using the invariant grid. Similarly to the pressure populations, the mirror-bounce back scheme equation (49) is adopted in order to impose symmetry condition on the vertical boundaries of the domain. Usual bounce-back condition (51) is used for simulating the adiabatic wall of the nozzle, while the equilibrium populations corresponding to the fresh mixture computed with a fixed parabolic velocity profile are maintained at the inlet. Finally, at the outlet, we make use of the following extrapolation:

$$\xi^i_\alpha(i, N_y) = \xi^i_\alpha(i, N_y - 1), \quad i = 1, \ldots, N_x. \tag{52}$$

Here, the species mass fraction and the temperature field, along the nozzle centerline, are shown in Figure 7, whereas in Figures 8 and 9 we report a sequence of snapshots of the time and space evolution of the O radical. It has been demonstrated (Chiavazzo *et al.*, 2009) that the above methodology for model reduction is indeed able to reproduce results of the detailed model in Section 3 with great accuracy when dealing with one-dimensional flames of air and hydrogen. Nevertheless, it is worth noticing that results of the present study have been obtained at a fraction of the cost required to solve the full set of equations of Section 3. First of all, the major drawback of LB solvers for reactive flows, namely the huge number of fields to solve for and store in the memory, is addressed: in the present case only one quarter of the fields are taken into account. To this respect, the savings in terms of memory and computational time can become even more significant, as soon as we start dealing with detailed hydrocarbon mechanisms where the number of degrees of freedom are much larger (typically hundreds of chemical species are involved in a reaction).

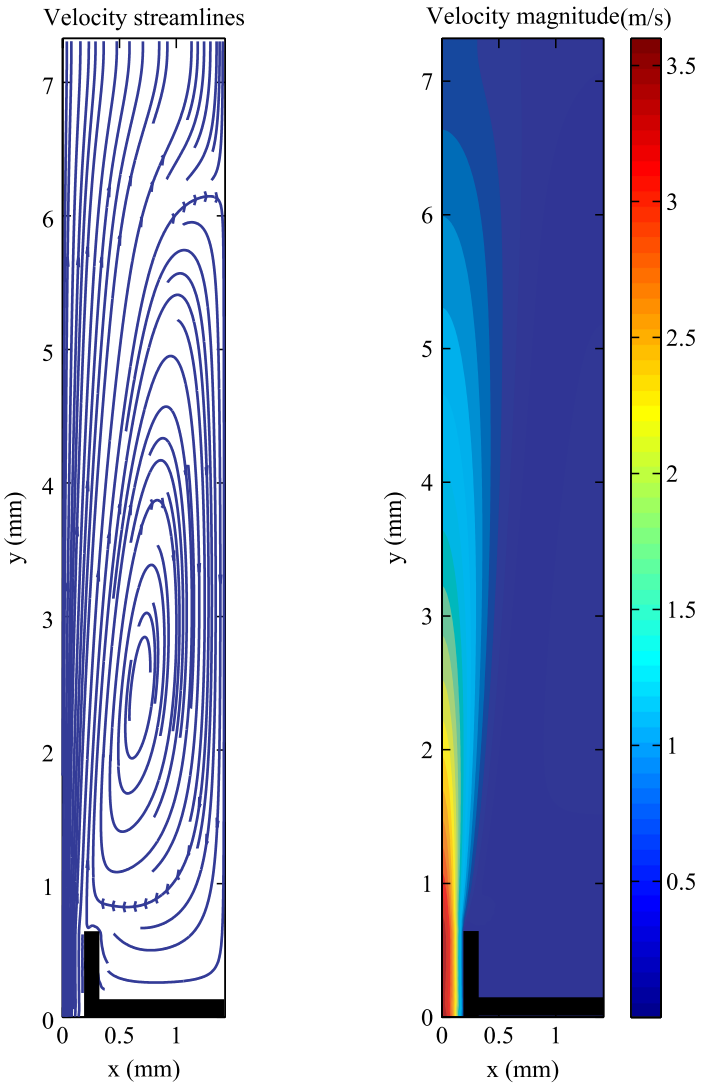

Figure 6.
Streamlines and Euclidean norm of the velocity field in the computational domain after 120,000 LB steps

Moreover, the chemical source terms introduce stiffness in the species equations (14), hence their solution requires a sufficiently short time step δt, able to describe the fastest time scale in the problem. In particular, an estimate of time scales, due to chemistry, can be found performing an eigenvalue analysis of the Jacobian matrix $\boldsymbol{J} = \left[\partial f_i / \partial Y_j\right]$. In our case, the matrix $\boldsymbol{J}$ computed at the steady state condition (fully burned mixture) exhibits the following time scales $|1\lambda_i|$:

$$\begin{aligned} &\frac{1}{|\lambda_1|} \simeq 2 \times 10^{-4}, \frac{1}{|\lambda_2|} \simeq 7.7 \times 10^{-6}, \frac{1}{|\lambda_3|} \simeq 4.4 \times 10^{-7}, \\ &\frac{1}{|\lambda_4|} \simeq 2.5 \times 10^{-7}, \frac{1}{|\lambda_5|} \simeq 2.2 \times 10^{-7}, \frac{1}{|\lambda_6|} \simeq 1.5 \times 10^{-7}, \end{aligned} \tag{53}$$

where $|\lambda_i|$ is the absolute value of an arbitrary non-zero eigenvalue of $\boldsymbol{J}$. Hence, when solving the detailed model of Section 3, the time step cannot be chosen larger than

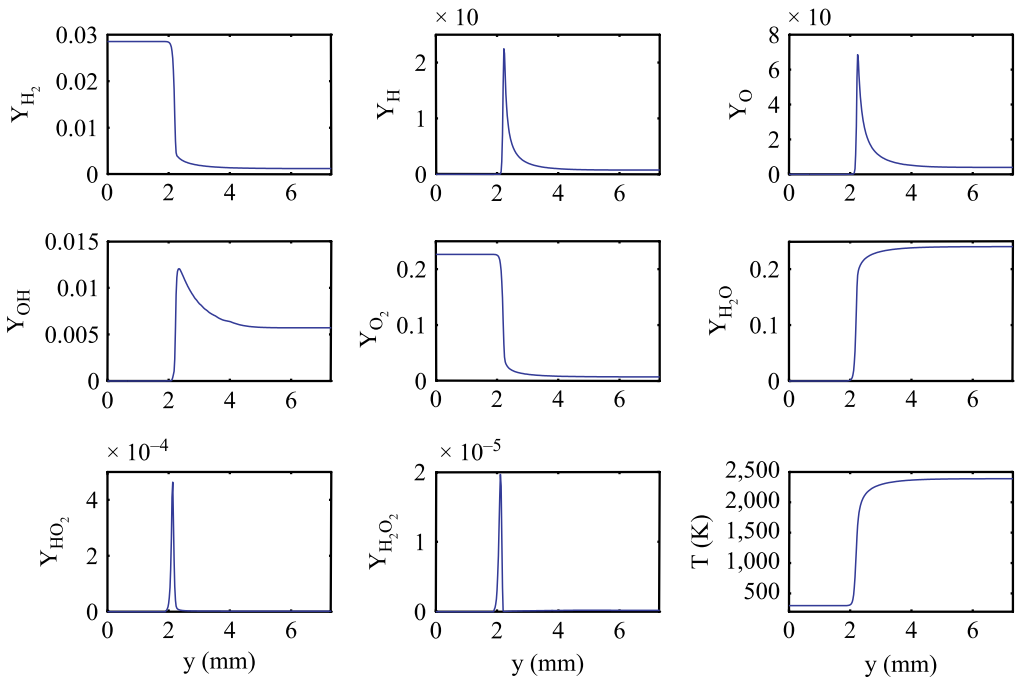

Figure 7.
Profiles of the species mass fraction and temperature along the nozzle centerline at the time instant $t = 2.2667$ ms

$\delta t \simeq 1 \times 10^{-7}$ s. Notice, however, that for the simulation results of Figures 7, 8 and 9, the technique suggested in Section 5 enables us to choose a time step $\delta t = 3 \times 10^{-6}$, with an additional saving of around thirty times in terms of computational time. Finally, the present setup has been computed on a single 2 GHz CPU double core with 4 GB RAM memory, and it takes 2.3 s in order to complete a time step: streaming, collision, rates computation and reaction sub-steps.

6. Discussion and outlook

It is worth noticing that, here the coupling of the model reduction procedure MIG and the LB model in Yamamoto *et al.* (2002) has been obtained, without loss of generality, under some assumptions, which can be gradually relaxed depending on the level of complexity that one can afford. Let us focus for now on low-Mach number combustion, where the total mixture pressure can be safely assumed constant. Above, we have considered the case of equal diffusivity and Lewis number $Le = 1$ for all the species: this guarantees that both the element mole numbers N_k in equation (11) and the mixture averaged enthalpy $\bar{h}$ remain constant in the domain. One more degree of freedom can be added to the problem, if we assume equal diffusivity for all the species with the Lewis number $Le \neq 1$. Now, the element composition is still conserved, while the enthalpy $\bar{h}$ varies in the domain according to the equation (19): the reduced model is fully described by the chemical coordinates ξ^i, the mixture enthalpy $\bar{h}$, and the construction, illustrated in Section 4 for batch reactors, is to be performed over a range of enthalpies. In the general case, also the element composition varies, due to differential diffusion effects, and additional equations for N_k shall be solved:

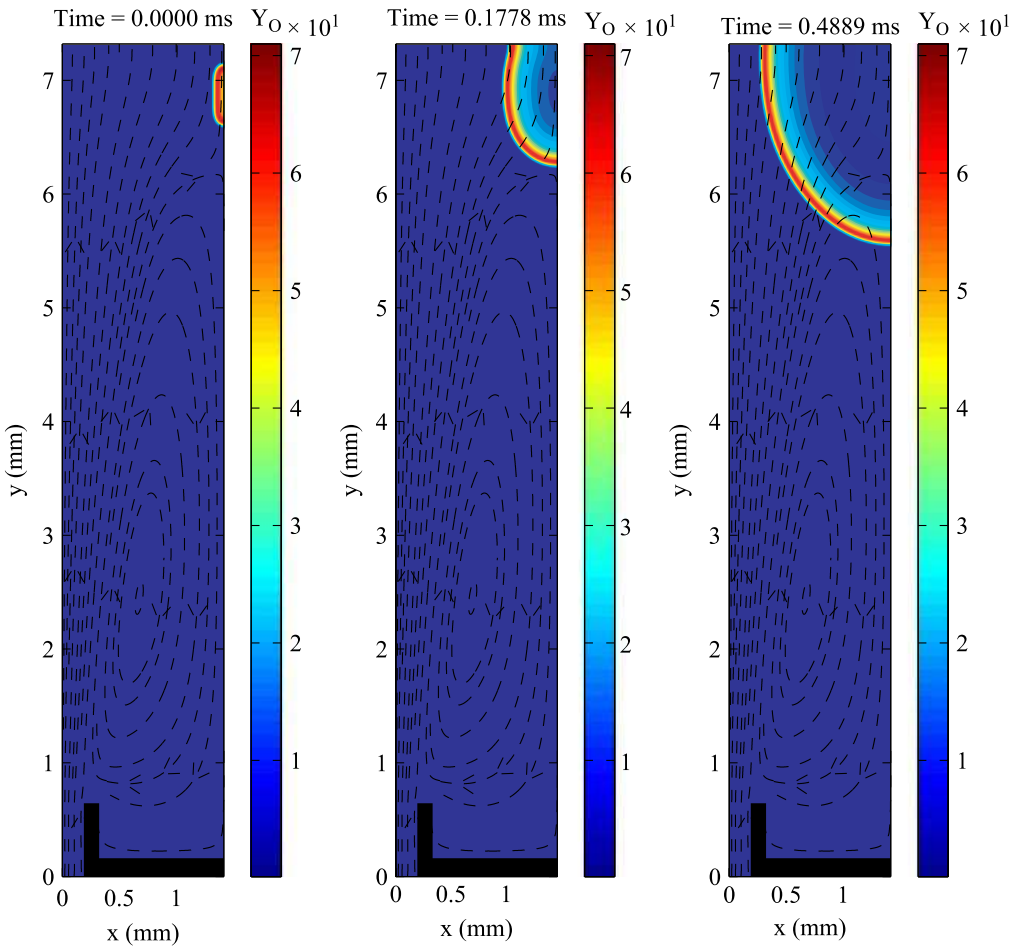

Figure 8.
Sequence of snapshots representing the time and space evolution of *O* radical

$$\bar{\rho}(\partial_t N_k + u_j \partial_j N_k) = \partial_j \left(\bar{\rho} \partial_j \left(\sum_{i=1}^{n} \frac{D_i \mu_{ik} Y_i}{W_i} \right) \right), \tag{54}$$

since the reduced model is completely described by the chemical coordinates ξ^i, $\bar{h}$ and N_k. The equation (54) can be also written in the diffusion, advection and reaction form (like equations (13) and (14)):

$$\bar{\rho}(\partial_t N_k + u_j \partial_j N_k) = \partial_j \left(\bar{\rho} \bar{D} k \partial_j N_k \right) + \partial_j \left(\bar{\rho} N_k \partial_j \bar{D} k \right), \tag{55}$$

where both the diffusion coefficient:

$$\bar{D}_k = \left(\sum\nolimits_{i=1}^{n} \frac{(D_i \mu_{ik} Y_i / W_i)}{N_k} \right) \tag{56}$$

and the source term $\partial_j \left(\bar{\rho} N_k \partial_j \bar{D} k \right)$ can be tabulated as functions of the grid parameters.

It has been found that the laminar flame speed s_L of the current setup is around 2.2 m/s, and it is in good agreement with experimental data (Chiavazzo *et al.* 2009). Hence, we would expect that, in the case discussed in section 5, the flame assumes the

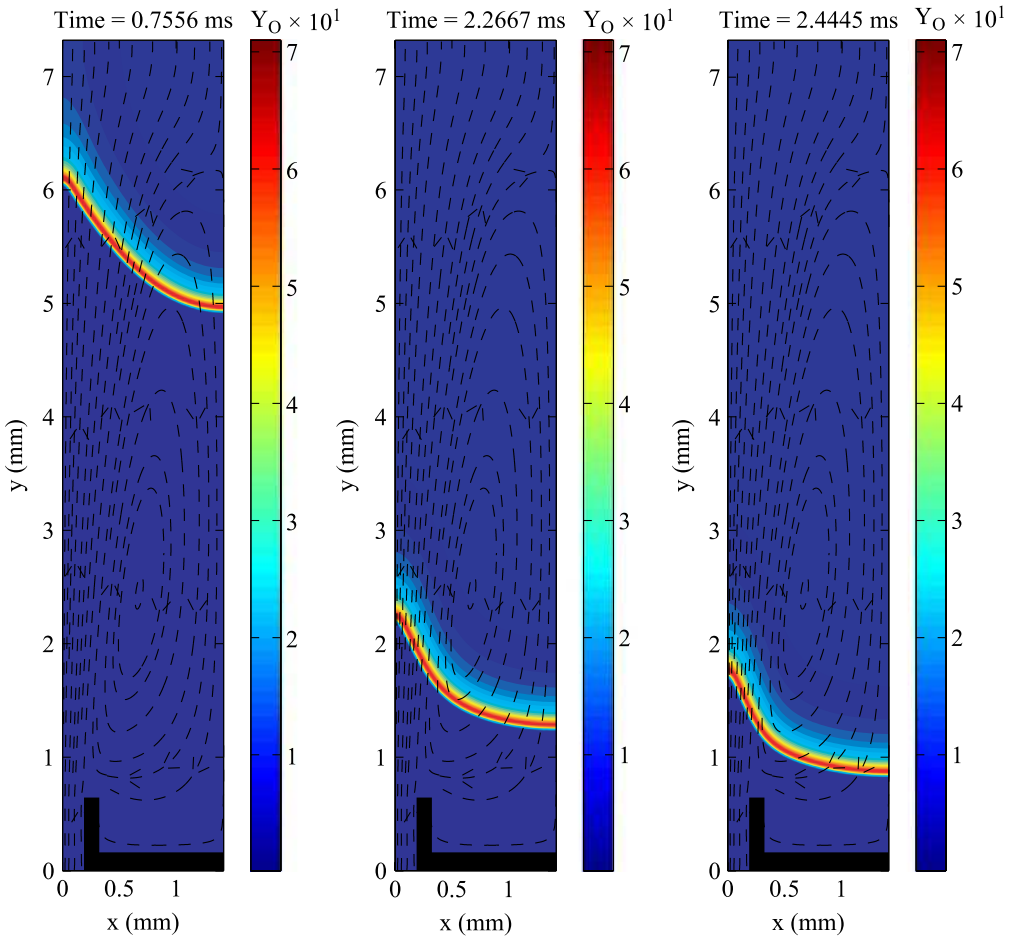

Figure 9.
Sequence of snapshots representing the time and space evolution of O radical

typical triangular shape with the uppermost vertex located on the nozzle centerline at around $y = 2.1$ mm, after stabilizing (Figures 9 and 10).

Nevertheless, we have noticed from the computations that, in a range of flow velocities ($u_{max} = 3.6 - 4.8$ m/s) and species diffusivity ($D = 2 \times 10^{-5} - 5 \times 10^{-5}$), the flame stabilization does not occur, while it proceed till the inlet. According to the cartoon in Figure 10, in a Bunsen burner, the stabilization of a flame front is expected at the points where the normal component of the upstream fluid velocity u_1 equals the laminar flame speed s_L, whereas the fluid flow is refracted after passing trough the flame and leaves at velocity u_2 (Law, 2006). In addition, heat losses in a vicinity of the nozzle wall do play an important role in the above phenomenon (Fiorina *et al.*, 2003), and this can be taken into account by considering the variations of the mixture enthalpy $\bar{h}$.

Obviously, the simple LB model described in Section 3 is not expected to correctly predict the above phenomenon, mainly due to the decoupling of the flow field from the chemical reaction, and the assumption of adiabatic flow. However, as illustrated in Section 6, the latter assumptions are not restricting, and more realistic reactive flows shall be simulated in the near future, where the incompressible description for the flow fields (12) and (15) is substituted with fully compressible models like the one suggested

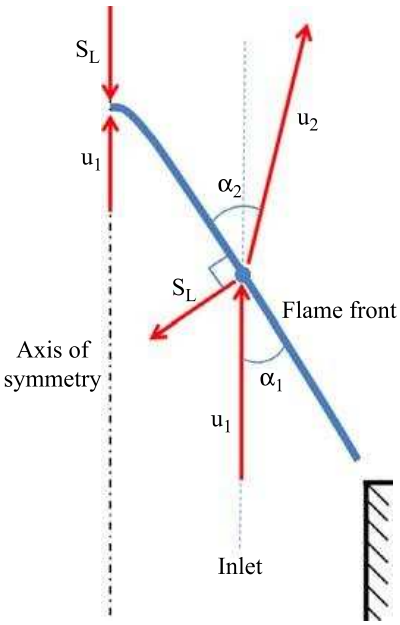

Note: The flame front stabilizes at the points where the normal component of the upstream fluid velocity u_1 equals the laminar flame speed s_L

Figure 10.
Illustration of a premixed flame in a Bunsen burner

in Prasianakis and Karlin (2007), while non-adiabatic conditions are taken into account by adding one more degree of freedom ($\bar{h}$) to the chemical parameters (ξ^i) of the table resulting from the reduced reaction mechanism.

7. Conclusions

Here, we illustrate a promising methodology for using accurate reduced chemical kinetics in combination with a LB solver in reactive flows simulations. It has been shown that the MIG is suitable for providing the reduced description of detailed chemistry, and this approach enables to cope with stiffness introduced by chemical source terms when solving species equations. Moreover, with the help of a 2D laminar flame computation, we have demonstrated that, model reduction procedures are twofold beneficial because they allow to both drastically increase the time step and reduce the number of fields to solve for: The above features are particularly desirable in the LBM, where the number of fields is significantly larger than conventional methods, and explicit time scheme is adopted. Finally, possible extensions and improvements to the current study are worked out.

References

Arcidiacono, S., Karlin, I.V., Mantzaras, J. and Frouzakis, E. (2007), "Lattice Boltzmann model for the simulation of multicomponent mixtures", *Phys. Rev. E*, Vol. 76, p. 046703.

Asinari, P. (2009), "Lattice Boltzmann scheme for mixture modeling: analysis of the continuum diffusion regimes recovering Maxwell-Stefan model and incompressible Navier-Stokes equations", *Phys. Rev. E*, Vol. 80.

Borok, S., Goldfarb, I. and Gol'dshtein, V. (2008), "About non-coincidence of invariant manifolds and intrinsic low dimensional manifolds (ILDM)", *Comm. Nonlinear Sci. and Num. Simul.*, Vol. 13, pp. 1029-38.

Bykov, V.I., Yablonskii, G.S. and Akramov, T.A. (1977), "The rate of the free energy decrease in the course of the complex chemical reaction", *Dokl. Akad. Nauk. SSSR* (*DokladyChemistry*), Vol. 234 No. 3, pp. 621-34.

Chapman, S. and Cowling, T.G. (1970), *The Mathematical Theory of Non-uniform Gases*, Cambridge University Press, Cambridge.

Chen, S. and Doolen, G. (1998), "Lattice Boltzmann method for fluid flows", *Annu. Rev. Fluid Mech.*, Vol. 30, pp. 329-64.

Chiavazzo, E. (2009), "Invariant manifolds and lattice boltzmann method for combustion", PhD thesis 18233, Swiss Federal Institute of Technology (ETH), Zurich.

Chiavazzo, E. and Karlin, I.V. (2008), "Quasi-equilibrium grid algorithm: Geometric construction for model reduction", *Jour. Comput. Phys.*, Vol. 227, pp. 5535-60.

Chiavazzo, E., Karlin, I.V. and Gorban, A. (2010), "The role of thermodynamics in model reduction when using invariant grids", *Comm. Comput. Phys.*, Vol. 8, pp. 701-34.

Chiavazzo, E., Gorban, A.N. and Karlin, I.V. (2007), "Comparison of invariant manifolds for model reduction in chemical kinetics", *Comm. Comput. Phys.*, Vol. 2, pp. 964-92.

Chiavazzo, E., Karlin, I.V., Frouzakis, C.E. and Boulouchos, K. (2009), "Method of invariant grid for model reduction of hydrogen combustion", *Proc. Combust. Instit.*, Vol. 32, pp. 519-26.

Chiavazzo, E., Karlin, I.V., Gorban, A.N. and Boulouchos, K. (2009), "Combustion simulation via lattice Boltzmann and reduced chemical kinetics", *J. Stat. Mech.: Theory and Exp*, p. P06013.

Dimitrov, V.I. (1977), "The maximum kinetic mechanism and rate constants in the H_2-O_2 system", *Reaction Kinetics and Catalysis Letter*, Vol. 7 No. 1, pp. 111-4.

Duchene, P. and Rouchon, P. (1996), "Kinetic scheme reduction via geometric singular perturbation techniques", *Chem. Eng. Sci.*, Vol. 51, pp. 4661-72.

Fiorina, B., Baron, R., Gicquel, O., Thevenin, D., Carpentier, S. and Darabiha, N. (2003), "Modelling non-adiabatic partially premixed flames using flame-prolongation of ILDM", *Combust. Theory Modelling*, Vol. 7, pp. 449-70.

Frouzakis, C.E. and Boulouchos, K. (2000), "Analysis and reduction of the CH4-air mechanism at lean conditions", *Comb. Sci. Tech.*, Vol. 159, pp. 281-303.

Gorban, A. and Karlin, I.V. (1992), "Thermodynamic parameterization", *Physica A*, Vol. 190, pp. 393-404.

Gorban, A. and Karlin, I.V. (2005), *Invariant Manifolds for Physical and Chemical Kinetics*, Springer, Berlin.

Gorban, A.N., Karlin, I.V. and Zinovyev, A.Y. (2004), "Invariant grids for reaction kinetics", *Physica A: Statistical and Theoretical Physics*, Vol. 333, pp. 106-54.

Hamiroune, H., Bishnu, P., Metghalchi, M. and Keck, J.C. (1998), "Rate-controlled constrained-equilibrium method using constraint potentials", *Combust. Theory Model.*, Vol. 2, pp. 81-94.

Karlin, I.V., Ferrante, A. and Öttinger, H.C. (1999), "Perfect entropy functions of the lattice Boltzmann method", *Europhys. Lett.*, Vol. 47 No. 2, pp. 182-8.

Keck, J.C. and Gillespie, D. (1971), "Rate-controlled partial-equilibrium method for treating reacting gas-mixtures", *Combust. Flame*, Vol. 17, pp. 237-41.

Lam, S.H. and Goussis, D.A. (1994), "The CSP method for simplifying kinetics", *Int. J. Chem. Kinet.*, Vol. 26, pp. 461-86.

Law, C.K. (2006), *Combustion Physics*, Cambridge University Press, Cambridge, pp. 263-5.

Lebiedz, D. (2004), "Computing minimal entropy production trajectories: an approach to model reduction in chemical kinetics", *Jour. Chem. Phys.*, Vol. 120, pp. 6890-7.

Li, J., Zhao, Z., Kazakov, A. and Dryer, F.L. (2004), "An updated comprehensive kinetic model of hydrogen combustion", *Int. J. Chem. Kinet.*, Vol. 36, pp. 566-75.

Maas, U. and Pope, S.B. (1992), "Simplifying chemical kinetics: intrinsic low-dimensional manifolds in composition space", *Combust. Flame*, Vol. 88, pp. 239-64.

Prasianakis, N. and Karlin, V. (2007), "Lattice boltzmann method for thermal flow simulation on standard lattices", *Phys. Rev. E*, Vol. 76, p. 016702.

Rabitz, H. (1987), "Chemical dynamics and kinetics phenomena as revealed by sensitivity analysis techniques", *Chem. Rev*, Vol. 87, pp. 101-12.

Ren, Z., Pope, S.B., Vladimirsky, A. and Guckenheimer, J.M. (2006), "The invariant constrained equilibrium edge preimage curve method for the dimension reduction of chemical kinetics", *Jour. Chem. Phys.*, Vol. 124, pp. 111-4.

Roussel, M.R. and Fraser, S.J. (1993), "Global analysis of enzyme inhibition kinetics", *J. Phys. Chem.*, Vol. 97, pp. 8316--8327.

Singh, S., Powers, J.M. and Paolucci, S. (2002), "On slow manifolds of chemically reactive systems", *J. Chem. Phys.*, Vol. 117, pp. 1482--1496.

Succi, S. (2001), *The Lattice Boltzmann Equation for Fluid Dynamics and Beyond*, Oxford University Press, Oxford.

Tang, Q. and Pope, S.B. (2004), "A more accurate projection in the rate-controlled constrained-equilibrium method for dimension reduction of combustion chemistry", *Combust. Theory Model.*, Vol. 8, pp. 255-79.

Yamamoto, K., He, X. and Doolen, G.D. (2002), "Simulation of combustion fields with lattice boltzmann method", *Jour. Stat. Phys.*, Vol. 107, pp. 367-83.

Further reading

Bhatnagar, P.L., Gross, E.P. and Krook, M. (1954), "A model for collision processes in gases. I. small amplitude processes in charged and neutral one-component systems", *Phys. Rev.*, Vol. 94 No. 3, pp. 511-25.

Corresponding author

Eliodoro Chiavazzo can be contacted at: eliodoro.chiavazzo@polito.it